BJR

Received: 9 November 2014 | Revised: 9 January 2015 | Accepted: 20 January 2015

doi: 10.1259/bjr.20140738

Cite this article as:
Ueno Y, Takahashi S, Ohno Y, Kitajima K, Yui M, Kassai Y, et al. Computed diffusion-weighted MRI for prostate cancer detection: the influence of the combinations of *b*-values. Br J Radiol 2015;88:20140738.

FULL PAPER

Computed diffusion-weighted MRI for prostate cancer detection: the influence of the combinations of *b*-values

[1]Y UENO, MD, PhD, [1]S TAKAHASHI, MD, PhD, [1,2]Y OHNO, MD, PhD, [1]K KITAJIMA, MD, PhD, [3]M YUI, MS, [3]Y KASSAI, MS, [4]F KAWAKAMI, MD, [5]H MIYAKE, MD, PhD and [1]K SUGIMURA, MD, PhD

[1]Department of Radiology, Kobe University Graduate School of Medicine, Kobe, Japan
[2]Advanced Biomedical Imaging Research, Kobe University Graduate School of Medicine, Kobe, Japan
[3]Toshiba Medical Systems Corporation, Otawara, Tochigi, Japan
[4]Department of Pathology, Kobe University Graduate School of Medicine, Kobe, Japan
[5]Department of Urology, Kobe University Graduate School of Medicine, Kobe, Japan

Address correspondence to: Dr Yoshiko Ueno
E-mail: *yonu0121@yahoo.co.jp*

Objective: To evaluate the influence of the combinations of *b*-values on computed diffusion-weighted images (cDWIs) for prostate cancer (PCa) detection at $b = 2000\ s\ mm^{-2}$.
Methods: Diffusion-weighted imaging (DWIs) for 31 patients with PCa (65.2 ± 7.1 years) were obtained pre-operatively at different *b*-values (0, 100, 500, 1000 and $2000\ s\ mm^{-2}$) on a 3-T MRI. cDWIs at $b = 2000$ were generated by using six *b*-value combinations: 0–100 $s\ mm^{-2}$ ($cDWI_{0–100}$); 0–500 $s\ mm^{-2}$ ($cDWI_{0–500}$); 100–500 $s\ mm^{-2}$ ($cDWI_{100–500}$); 0–1000 $s\ mm^{-2}$ ($cDWI_{0–1000}$); 100–1000 $s\ mm^{-2}$ ($cDWI_{100–1000}$); and 500–1000 $s\ mm^{-2}$ ($cDWI_{500–1000}$). These cDWIs and measured DWIs with $b = 2000\ s\ mm^{-2}$ ($mDWI_{2000}$) were evaluated in this setting. To assess image quality for each DWI, contrast ratios (CRs) of cancerous and non-cancerous lesions were evaluated. To compare the detectability of PCa for each DWI, receiver operating characteristic analysis was used.
Results: CRs of all cDWIs were significantly higher than those of $mDWI_{2000}$ ($p < 0.05$). Areas under the curve of $cDWI_{0–100}$ (0.62) and $cDWI_{0–500}$ (0.65) were significantly smaller ($p < 0.05$) than those of others ($cDWI_{100–500}$, 0.72; $cDWI_{0–1000}$, 0.73; $cDWI_{100–1000}$, 0.71; $cDWI_{500–1000}$, 0.74; $mDWI_{2000}$, 0.72).
Conclusion: The combinations of *b*-values influenced image quality and diagnostic ability of cDWIs for PCa detection. The combinations of $b \geq 100$ and $b \geq 500\ s\ mm^{-2}$, as well as $b = 0$ and $b = 1000\ s\ mm^{-2}$, were optimal in this study.
Advances in knowledge: For generating the useful cDWI for PCa detection, radiologists should take care of the combination of *b*-values when including low *b*-values.

Diffusion-weighted imaging (DWI) and MRI are now being widely used in body cancer imaging for detection, characterization and assessment of treatment response.[1–3] Prostate cancer (PCa) detection is sometimes difficult because of the high background signal of parenchyma due to the presence of hypertrophy, bleeding and inflammation.

Therefore, for better cancer detection with DWI, the focus should be on contrast in signal intensity (SI) between cancer and normal parenchyma.[4,5] It has recently been reported that DWI obtained with ultrahigh *b*-values provide good contrast between cancerous and background tissue for better PCa detection.[6–8] Furthermore, two studies in particular have demonstrated the advantage of DWI obtained with a *b*-value of $2000\ s\ mm^{-2}$ rather than with $1000\ s\ mm^{-2}$ for PCa diagnosis using either 1.5- or 3.0-T MR systems.[8,9] These studies found that the background tissue signal on DWI obtained with $2000\ s\ mm^{-2}$ is more suppressed and the contrast between signals of cancerous and non-cancerous lesions thus more enhanced than on DWI obtained with $1000\ s\ mm^{-2}$. Although images obtained with *b*-values $>1000\ s\ mm^{-2}$ are clinically preferable, they are more difficult to obtain in practice because of certain disadvantages such as poor signal-to-noise ratio (SNR) and potential eddy current distortions resulting from the large diffusion-sensitizing gradients used.

Computed DWI (cDWI) is a recently introduced computational technique that can produce any *b*-value images from DWI acquired with at least two different *b*-values.[10–12] Blackledge et al have proved that the cDWI technique allows higher *b*-value images to be obtained with a good SNR because it can suppress background noise while maintaining the original lesion signal. Furthermore, cDWI generated at $b = 2000\ s\ mm^{-2}$ from DWI obtained with $b = 0$ and $1000\ s\ mm^{-2}$ reportedly attained a better contrast ratio (CR) between cancerous and non-cancerous lesions than did an actual DWI measured with $b = 2000\ s\ mm^{-2}$

and showed a detection ability for PCa comparable to that of an actual DWI measured with $b = 2000\,s\,mm^{-2}$.[13] However, it remains unclear which combination of b-values is optimal for generating cDWI with a high b-value such as $2000\,s\,mm^{-2}$ for detection of PCa in routine clinical practice. The aim of our study was therefore to evaluate the influence of the combinations of b-values on cDWI at $b = 2000\,s\,mm^{-2}$ for PCa detection and to determine the optimal combination on a 3-T MR system.

METHODS AND MATERIALS

Patients

Our retrospective study was approved by our institute's ethics committee (Kobe University Graduate School of Medicine), and written informed consent was waived. A total of 45 consecutive patients with biopsy-proven PCa underwent 3-T MRI examinations, including DWI, of the prostate followed by radical prostatectomy between June 2012 and January 2013. 14 patients were excluded for having been treated with hormone and/or radiation therapy instead of surgery. The remaining 31 patients formed the study group (mean age, 65.2 ± 7.1 years). Details of patient characteristics are shown in Table 1.

MRI

All MR examinations were performed with the aid of a 3-T MR unit (Achieva®; Philips Healthcare, Best, Netherlands) using a multichannel phased-array coil (SENSE Cardiac 6ch-coil; Philips Healthcare) with parallel imaging capability. No endorectal coil was used. The maximal gradient specifications were $100\,mT\,m^{-1}$ (for DWI) and $40\,mT\,m^{-1}$ (for other sequences) for amplitude and $80\,mT\,m^{-1}\,ms^{-1}$ (for DWI) and $200\,mT\,m^{-1}\,ms^{-1}$ (for other sequences) for the slew rate. T_2 weighted (T2W) turbo spin-echo images, covering the entire prostate gland and seminal vesicles, were acquired in two orthogonal planes, axial and coronal. The acquisition parameters for T2W images and diffusion-weighted (DW) images are shown in Table 2. T_1 weighted images and dynamic contrast-enhanced images were also obtained for clinical examinations, but they were not evaluated for this study. Peristalsis was suppressed with intramuscular administration of 20 mg of scopolamine butylbromide (Buscopan®; Nippon Boehringer Ingelheim, Yamagata, Japan) or 1 mg of glucagon (Glucagon-G Novo; Eisai Co. Ltd, Tokyo, Japan).

Computed diffusion-weighted imaging

Using two measured DWI signals, the apparent diffusion coefficient (ADC) was calculated on the basis of a mono-exponential model with the formula: $ADC = \ln(-S_1/S_2)/(b_1-b_2)$, where S_1 is SI for $b = b_1$ and S_2 is SI for $b = b_2$. ADC maps were constructed with the same equation but on the basis of a voxel-wise calculation. The computed DWI signal for $b = b_c$ was then obtained with the equation $S_c = S_1 \exp[-(b_c-b_1)ADC]$.[10–12]

Computed DW MR images at $b = 2000\,s\,mm^{-2}$ were generated from the following six b-value combinations: (1) between 0 and $100\,s\,mm^{-2}$, $cDWI_{0–100}$; (2) between 0 and $500\,s\,mm^{-2}$, $cDWI_{0–500}$; (3) between 100 and $500\,s\,mm^{-2}$, $cDWI_{100–500}$; (4) between 0 and $1000\,s\,mm^{-2}$, $cDWI_{0–1000}$; (5) between 100 and $1000\,s\,mm^{-2}$, $cDWI_{100–1000}$; and (6) between 500 and $1000\,s\,mm^{-2}$, $cDWI_{500–1000}$. Matrix laboratory-based research software, the cDWI calculator (Toshiba Medical Systems Corporation, Otawara, Japan), was used on a personal computer for generating all computed DW images at 3 s per slice.

Pathological analysis

The presence of PCa in all 31 patients was proven histopathologically after radical prostatectomy. Prostatectomy specimens were marked with ink, fixed overnight in 10% buffered formalin and sliced from the apex to the base at 3- to 4-mm intervals. All glass slides obtained from the pathological step-section slices were reviewed by a board-certified pathologist (FK) with 10 years' experience, who was blinded to the MRI findings. For region-specific comparisons among the protocols, the prostate was divided into eight regions: the bilateral peripheral zones (PZs) comprising the base, midgland and the apex, and the bilateral transition zones (TZs). For determining radiological–pathological correlations, a region was considered positive for cancer if it contained a cancer regardless of its diameter. The locations of all tumour foci were recorded on a standardized diagram of the prostate.

Image analysis

Quantitative image analysis

The acquired images including real-measured DWI with $b = 2000\,s\,mm^{-2}$ ($mDWI_{2000}$) and all cDWIs were anonymized and collected in the digital imaging and communications in medicine (DICOM) format. Two board-certified genitourinary radiologists, one with 8 years' experience (YU) and the other with 13 years' experience (KK), who had no knowledge of either the histopathological findings or the clinical data, analysed the images. First, circular regions of interest (ROIs), created with DICOM viewers (ImageJ; US National Institutes of Health, Bethesda, MD), were placed on each $mDWI_{2000}$ by the two radiologists in consensus and

Table 1. Characteristics of the study subjects

Age (years)	
Mean and SD	65.2 ± 7.1
Range	51–81
Initial value of serum PSA ($ng\,ml^{-1}$)	
Mean and SD	8.56 ± 3.5
Range	4.7–16.5
Pathological stage	
pT2a	8
pT2b	8
pT2c	8
pT3a	6
pT3b	1
Highest Gleason score	
6 (3 + 3)	5
7 (4 + 3, 3 + 4)	16
8 (5 + 3, 4 + 4)	10

PSA, prostate-specific antigen; SD, standard deviation.

Table 2. MRI parameters

Parameter	T2WI (axial)	T2WI (coronal)	Diffusion-weighted imaging
Sequence	TSE	TSE	Single-shot EPI
Acquisition plane	Axial	Coronal	Axial
Repetition time/echo time (ms)	4000/130	3300/130	4000/65
Flip angle (°)	90	90	90
Echo train length/EPI factor	16	16	29
Sensitivity-encoding factor	2	2	3
Phase-encoding direction	RL	RL	AP
b-values (s mm^{-2})	–	–	0, 100, 500, 1000, 2000
Fat saturation	–	–	SPAIR
Field of view (mm)	200 × 200	200 × 200	450 × 360
Acquisition matrix	256 × 256	256 × 256	128 × 128
Slice thickness/gap (mm)	3/0	3/0	3/0
Number of slices	25	25	25
Number of excitations	3	3	3
Acquisition time (s)	3:40	2:30	7:20

AP, anterior to posterior; EPI, echo-planar imaging; RL, right to left; SPAIR, spectral attenuated with inversion recovery fat suppression method; T2WI, T_2 weighted imaging; TSE, turbo spin-echo.

within the malignant or normal lesions with reference to the histopathological findings of radical prostatectomy for each of the patients. The slice that includes the largest cancer cross section was selected for each patient. The same ROIs were then copied onto other DW images acquired in the same axial section. Finally, the mean signal intensities of both cancerous and non-cancerous lesions were measured on the DW images of all 31 patients. Then, the CR between cancerous and non-cancerous lesions was calculated with the following formula: $CR = (S_{ca} - S_{non\text{-}ca})/(S_{ca} + S_{non\text{-}ca})$, where S_{ca} is the average SI for the cancerous lesion and $S_{non\text{-}ca}$ is the average SI for the non-cancerous lesion. Finally, the CRs for the DW images were compared statistically.

Qualitative image analysis

For qualitative assessment, the images were visually checked and compared for the absence of geometric distortion, absence of image blurring, absence of ghost artefacts, clarity of prostate margin, lesion conspicuity and overall image quality. These parameters were scored with a five-point visual system by the two radiologists in consensus as follows: 5, excellent; 4, good; 3, moderate; 2, fair; and 1, poor. The parameter was scored as 0 when it was unevaluable. The evaluation scores for each of these items were then compared statistically among the DW images.

Detection capability assessment

To compare the capability of the DW images for facilitating detection, six combinations of images, Protocols A [T2W imaging (T2WI) + $cDWI_{0–100}$], B (T2WI + $cDWI_{0–500}$), C (T2WI + $cDWI_{100–500}$), D (T2WI + $cDWI_{0–1000}$), E (T2WI + $cDWI_{100–1000}$), F (T2WI + $cDWI_{500–1000}$) and G (T2WI + $mDWI_{2000}$), were independently evaluated by the same two genitourinary radiologists (YU and KK) for the likelihood of the presence of cancer by prostatic region. A five-point scale was used for evaluation: 5, definitely present; 4, probably present; 3, equivocal; 2, probably absent; 1, definitely absent. For region-specific comparisons among the protocols, the prostate was divided into the same eight regions as for the pathological analysis. Each data set was then independently reviewed by the two readers with a minimum interval of 1 month to avoid any decision threshold bias owing to reading-order effect. In addition, for both readers there was an interval of at least 1 week between quantitative and qualitative image analysis sessions. These assessments were performed before the previously mentioned quantitative and qualitative image analyses. The criteria for the diagnosis of PCa on each of the MR images were based on those used for several previous studies.[8,14–16] On T2WIs, a lesion in the PZ was considered to be definitely malignant if it showed homogeneous low SI with an irregular shape, unclear margin and diffuse extension with mass effect. As for the TZ, a mass showing a homogeneous low SI on the T2WI accompanied by destruction of normal structures, such as the surgical capsule or anterior fibromuscular stroma without a capsule, was considered to be definitely malignant. A lesion detected on DWI was considered malignant if it showed high intensity relative to the background prostate parenchyma.

For the standardization of these imaging assessments on DW images, the window width and window level were set at values according to each of the readers' preferred values for reading. Because this study focused on a comparison of the ability to enhance diagnostic accuracy and of image quality of the computed and acquired DW images, no ADC maps were used for visual assessments.

Statistical analysis

For quantitative assessment, CR from all DWI data sets were compared by means of Tukey–Kramer's test, as were visual scores for all DWI data sets for qualitative assessment.

For qualitative assessment of detection capability enhancement, interobserver agreement on the likelihood of the presence of cancer was assessed by means of κ statistics with quadratic weighting. A κ-value of up to 0.20 was considered to indicate slight agreement; 0.21–0.40, fair agreement; 0.41–0.60, moderate agreement; 0.61–0.80, substantial agreement; and ≥0.81, almost perfect agreement.[17]

Receiver operating characteristic (ROC) analyses were performed for comparison of detection capability accuracy for all protocols. The areas under the curves (Az) were estimated non-parametrically for ordinal score assessments and the findings of the ROC analyses were used to determine the threshold values. Finally, sensitivity, specificity, positive-predictive value, negative-predictive value and accuracy of the protocols were compared by means of the McNemar's test. These analyses were performed for whole prostate of all patients.

Commercially available software (JMP v. 9; SAS Institute Japan Ltd, Tokyo, Japan) was used for all statistical analyses. A two-tailed p-value of <0.05 was considered significant.

RESULTS

Histopathological examinations that identified 121 regions out of a total of 248 regions were found to be cancer positive (PZ, 94; TZ, 27).

The results of CR are shown in Figure 1. The CR of every computed DWI was significantly higher than that of $mDWI_{2000}$ ($cDWI_{0–100}$: 0.54 ± 0.30; $cDWI_{0–500}$: 0.40 ± 0.20; $cDWI_{100–500}$: 0.38 ± 0.20; $cDWI_{0–1000}$: 0.39 ± 0.20; $cDWI_{100–1000}$: 0.39 ± 0.10; $cDWI_{500–1000}$: 0.44 ± 0.20; $mDWI_{2000}$: 0.23 ± 0.1) ($p < 0.05$).

The visual assessment scores are shown in Table 3. On every $cDWI_{0–100}$, geometric distortion, image blurring and ghost artefacts were unevaluable, because the signal of the prostate was buried in the background signal. The visual score of $cDWI_{0–100}$ for every item was significantly lower than that of the other DW images ($p < 0.01$). Furthermore, visual scores for clarity of the prostate margin, lesion conspicuity and overall image quality of $cDWI_{0–500}$ were significantly lower than those of other DW images except for $cDWI_{0–100}$ ($p < 0.05$).

Table 4 shows the overall scores for assessment of probability of the presence of PCa on a per-region basis recorded by the two readers for each protocol. Interobserver agreement was rated as moderate for Protocols A (T2WI + $cDWI_{0–100}$), B (T2WI + $cDWI_{0–500}$), D (T2WI + $cDWI_{0–1000}$) and E (T2WI + $cDWI_{100–1000}$) and as substantial for Protocols C (T2WI + $cDWI_{100–500}$), F (T2WI + $cDWI_{500–1000}$) and G (T2WI + $mDWI_{2000}$).

The results of ROC analyses by Reader 1 (YU) are shown in Figure 2. The Az of Protocol A (0.62) was significantly smaller than that of the others (C: 0.72, $p = 0.01$; D: 0.73, $p = 0.005$; E: 0.71, $p = 0.005$; F: 0.74, $p = 0.008$; and G: 0.72, $p = 0.005$). Az of Protocol B (0.65) was also significantly smaller than C, D, E, F and G (C: $p = 0.04$; D: $p = 0.03$; E: $p = 0.04$; F: $p = 0.02$; and G: $p = 0.03$).

On the basis of the findings for ROC analyses, the threshold value for the visual scoring system for each protocol was set at three. Table 5 shows the diagnostic ratings for each protocol. The sensitivity of Protocols A (55.4%), B (49.6%) and C (59.5%) was

Figure 1. Comparisons of contrast ratio (CR) for each diffusion-weighted imaging (DWI). The CR for cancerous and non-cancerous lesions of each DWI. The CR of measured DWIs with $b = 2000\ s\ mm^{-2}$ ($mDWI_{2000}$) was significantly lower than that of all other computed DWIs (cDWIs). *$p < 0.05$, **$p < 0.01$. b-value combinations: 0–100 $s\ mm^{-2}$ ($cDWI_{0–100}$); 0–500 $s\ mm^{-2}$ ($cDWI_{0–500}$); 100–500 $s\ mm^{-2}$ ($cDWI_{100–500}$); 0–1000 $s\ mm^{-2}$ ($cDWI_{0–1000}$); 100–1000 $s\ mm^{-2}$ ($cDWI_{100–1000}$); 500–1000 $s\ mm^{-2}$ ($cDWI_{500–1000}$).

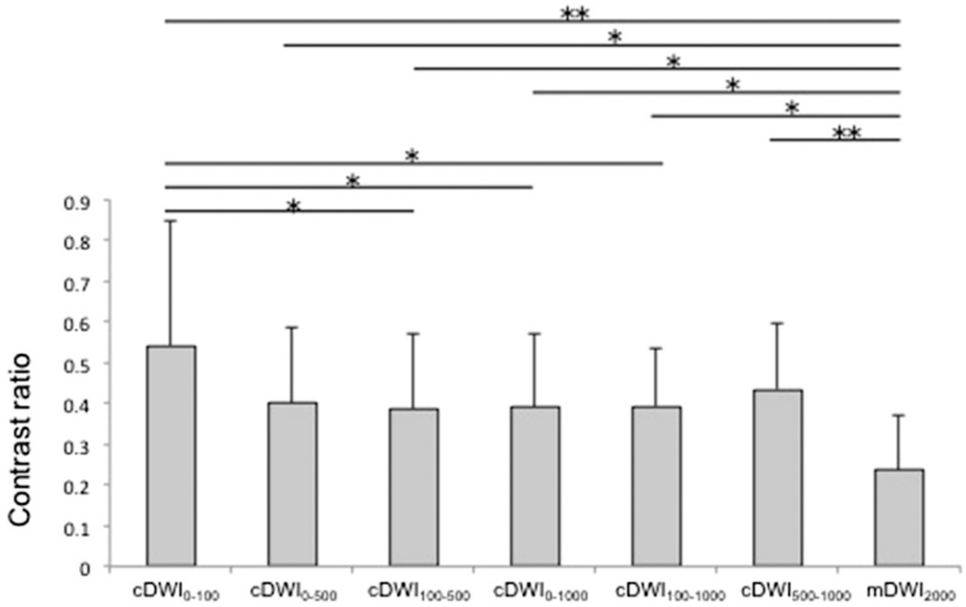

Table 3. Comparison of diffusion-weighted imaging (DWI) capability for qualitative assessments

Diffusion weighted images	Evaluation items					
	Absence of geometric distortion	Absence of image blurring	Absence of ghost artefacts	Clarity of prostate margin	Lesion conspicuity	Overall image quality
$cDWI_{0–100}$	0	0	0	1.14 ± 0.3	1.11 ± 0.3	1.00 ± 0.0
$cDWI_{0–500}$	3.33 ± 0.6	4.88 ± 0.5	4.80 ± 0.4	3.25 ± 0.8	3.08 ± 0.7	3.31 ± 0.7
$cDWI_{100–500}$	3.76 ± 0.6	4.88 ± 0.6	4.80 ± 0.4	3.29 ± 0.7	3.19 ± 0.9	3.51 ± 0.6
$cDWI_{0–1000}$	3.90 ± 0.5	4.91 ± 0.3	4.85 ± 0.3	3.88 ± 0.5	4.20 ± 0.7	4.22 ± 0.5
$cDWI_{100–1000}$	3.91 ± 0.6	4.91 ± 0.3	4.85 ± 0.3	3.88 ± 0.5	4.20 ± 0.8	4.20 ± 0.5
$cDWI_{500–1000}$	3.68 ± 0.7	4.91 ± 0.3	4.80 ± 0.3	3.71 ± 0.7	4.22 ± 0.8	4.00 ± 0.7
$mDWI_{2000}$	3.74 ± 0.5	4.88 ± 0.5	4.82 ± 0.4	3.68 ± 0.7	3.93 ± 0.9	4.11 ± 0.5

cDWI, computed diffusion-weighted imaging; $cDWI_{0–100}$, cDWI 0–100 s mm^{-2}; $cDWI_{0–500}$, cDWI 0–500 s mm^{-2}; $cDWI_{100–500}$, cDWI 100–500 s mm^{-2}; $cDWI_{0–1000}$, cDWI 0–1000 s mm^{-2}; $cDWI_{100–1000}$, cDWI 100–1000 s mm^{-2}; $cDWI_{500–1000}$, cDWI 500–1000 s mm^{-2}; $mDWI_{2000}$, measured DWIs with b = 2000 s mm^{-2}.

significantly lower than that of Protocols D, E, F and G (D: 77.7%, $p < 0.0001$; E: 79.3%, $p < 0.0001$; F: 71.0%, $p < 0.0001$; and G: 83.5%, $p < 0.0001$). The specificity of Protocol B (77.2%) was significantly higher than those of the other DW images (A: 63.0%, $p < 0.0001$; C: 74.0%, $p = 0.04$; D: 62.2%, $p < 0.0001$; E: 59.1%, $p < 0.0001$, F: 59.8%, $p < 0.0001$ and G: 50.4%, $p < 0.0001$). The accuracy of Protocol A (59.3%) was significantly lower than that of Protocols C, D, E, F and G (C: 66.9%, $p = 0.03$; D: 69.8%, $p < 0.001$; E: 69.0%, $p = 0.01$; F: 65.3%, $p = 0.01$ and G: 61.5%, $p = 0.02$). A representative case is shown in Figure 3.

DISCUSSION

The aim of this study was to evaluate the influence of the combination of *b*-values on cDWI at $b = 2000$ s mm^{-2} for PCa detection and to determine the optimal combination on a 3-T MR system. Our findings suggest that, the combinations of *b*-value influenced the image quality and diagnostic ability of cDWI for PCa detection. Furthermore, it was suggested that the combinations of $b \geq 100$ and $b \geq 500$ s mm^{-2}, and $b = 0$ and $b = 1000$ mm^{-2} were optimal for cDWI generation.

Table 4. MRI scores and reader agreement for assessment of probability of presence of prostate cancer

Protocol	Reader	MRI score					κ value
		1	2	3	4	5	
A: T2WI + $cDWI_{0–100}$	1	36	105	70	26	10	0.50 (0.33, 0.65)
	2	54	81	71	23	20	
B: T2WI + $cDWI_{0–500}$	1	54	105	45	24	20	0.54 (0.37, 0.70)
	2	36	106	69	27	10	
C: T2WI + $cDWI_{100–500}$	1	50	93	31	47	27	0.63 (0.52, 0.75)
	2	36	104	67	24	10	
D: T2WI + $cDWI_{0–1000}$	1	34	72	63	51	28	0.58 (0.40, 0.72)
	2	26	74	79	45	24	
E: T2WI + $cDWI_{100–1000}$	1	20	77	57	55	39	0.60 (0.44, 0.76)
	2	24	60	87	51	26	
F: T2WI + $cDWI_{500–1000}$	1	22	94	53	41	38	0.64 (0.48, 0.80)
	2	13	96	71	40	28	
G: T2WI + $mDWI_{2000}$	1	15	76	80	50	27	0.62 (0.46, 0.77)
	2	13	40	119	41	35	

cDWI, computed diffusion-weighted imaging; $cDWI_{0–100}$, cDWI 0–100 s mm^{-2}; $cDWI_{0–500}$, cDWI 0–500 s mm^{-2}; $cDWI_{100–500}$, cDWI 100–500 s mm^{-2}; $cDWI_{0–1000}$, cDWI 0–1000 s mm^{-2}; $cDWI_{100–1000}$, cDWI 100–1000 s mm^{-2}; $cDWI_{500–1000}$, cDWI 500–1000 s mm^{-2}; DWI, diffusion-weighted imaging; $mDWI_{2000}$, measured DWIs with b = 2000 s mm^{-2}; T2WI, T_2 weighted imaging.
Figures in parentheses show 95% confidence intervals.

Figure 2. Receiver operating characteristic curves for prostate cancer diagnosis components of the seven protocols. Area under the curves (Az) of $cDWI_{0-100}$ (a) and $cDWI_{0-500}$ (b) was significantly smaller than that of the other diffusion-weighted images [(c), $cDWI_{100-500}$; (d), $cDWI_{0-1000}$; (e), $cDWI_{100-1000}$; (f), $cDWI_{500-1000}$; (g): $mDWI_{2000}$].

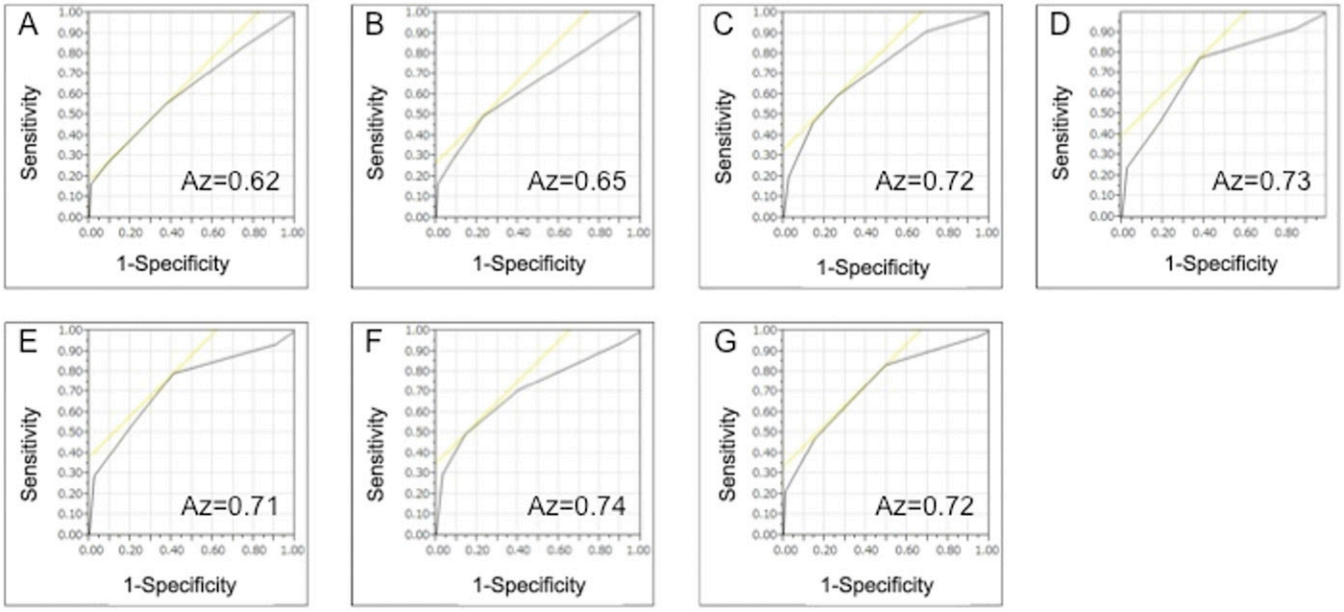

The computed DWI theory underlying our study is based on calculating ADC with a monoexponential model. The monoexponential model is simpler to perform, and the evidence is that it performs as well or almost as well as the biexponential model for cDWI theory.[18] Thus, optimization of computed DWI with the aid of a monoexponential model is especially relevant for clinical application.

This study has demonstrated that a better CR can be obtained with every computed DWI than with the directly measured DWI on a 3 T MRI. This finding agrees with the results of previously reported studies.[10–13] Blackledge et al[10] performed a copper sulfate phantom study and found that the noise remains constant across *b*-values for acquired images, whereas for computed images, it decreases when the *b*-value increases to $>840\ s\ mm^{-2}$. Computed DWI images are thus more likely than acquired images to highlight differences in SI between cancerous and non-cancerous tissue on images with high *b*-values. Our study confirmed that computed images yielded a better CR than actual-measure images with high *b*-values.

Table 5. Comparison of diagnostic performance of all methods

Protocol	Sensitivity (%)	Specificity (%)	Accuracy (%)	Positive-predictive value (%)	Negative-predictive value (%)	Area under the curve
A: T2WI + $cDWI_{0-100}$	55.4 (67/121)	63.0 (80/127)	59.3 (147/248)	58.8 (67/114)	59.7 (80/134)	0.62 (0.55, 0.69]
B: T2WI + $cDWI_{0-500}$	49.6 (60/121)	77.2 (98/127)	63.7 (158/248)	67.4 (60/89)	61.6 (98/159)	0.65 [0.58, 0.71]
C: T2WI + $cDWI_{100-500}$	59.5 (72/121)	74.0 (94/147)	66.9 (166/248)	68.6 (72/105)	65.7 (94/143)	0.72 [0.65, 0.78]
D: T2WI + $cDWI_{0-1000}$	77.7 (94/121)	62.2 (79/127)	69.8 (173/248)	66.2 (94/142)	74.5 (79/106)	0.73 [0.66, 0.79]
E: T2WI + $cDWI_{100-1000}$	79.3 (96/121)	59.1 (75/147)	69.0 (171/248)	64.9 (96/148)	75.0 (75/100)	0.71 [0.65, 0.77]
F: T2WI + $cDWI_{500-1000}$	71.1 (86/121)	59.8 (76/127)	65.3 (162/148)	62.8 (86/137)	68.5 (76/111)	0.74 [0.67, 0.79]
G: T2WI + $mDWI_{2000}$	83.5 (101/121)	50.4 (64/127)	66.5 (165/148)	61.6 (101/164)	76.2 (64/84)	0.72 [0.66, 0.78]

cDWI, computed diffusion-weighted imaging; $cDWI_{0-100}$, cDWI 0–100 $s\ mm^{-2}$; $cDWI_{0-500}$, cDWI 0–500 $s\ mm^{-2}$; $cDWI_{100-500}$, cDWI 100–500 $s\ mm^{-2}$; $cDWI_{0-1000}$, cDWI 0–1000 $s\ mm^{-2}$; $cDWI_{100-1000}$, cDWI 100–1000 $s\ mm^{-2}$; $cDWI_{500-1000}$, cDWI 500–1000 $s\ mm^{-2}$; DWI, diffusion-weighted imaging; $mDWI_{2000}$, measured DWIs with $b = 2000\ s\ mm^{-2}$; T2WI, T_2 weighted imaging.
Figures in parentheses show actual numbers. Figures in brackets show 95% confidence intervals.

Figure 3. A 68-year-old patient with prostate cancer (PCa) with Gleason score 4 + 3 = 7 PCa, pT3a, initial prostate-specific antigen of 7.8 ng ml^{-1}. On T_2 weighted imaging (a), both sides of the peripheral zone (PZ) show diffuse low intensity (arrowheads). On $cDWI_{0–100}$ (b) and $cDWI_{0–500}$ (c), no abnormal signal intensity suspicious for cancer was detected (arrowheads). Abnormal signal intensities (arrowheads) in the right and left lobes of the PZ are visible on $cDWI_{100–500}$ (d), $cDWI_{0–1000}$ (e), $cDWI_{100–1000}$ (f) $cDWI_{500–1000}$ (g) and $mDWI_{2000}$ (h). Pathological specimen examination confirmed PCa in the right and left lobes of the PZ (not shown).

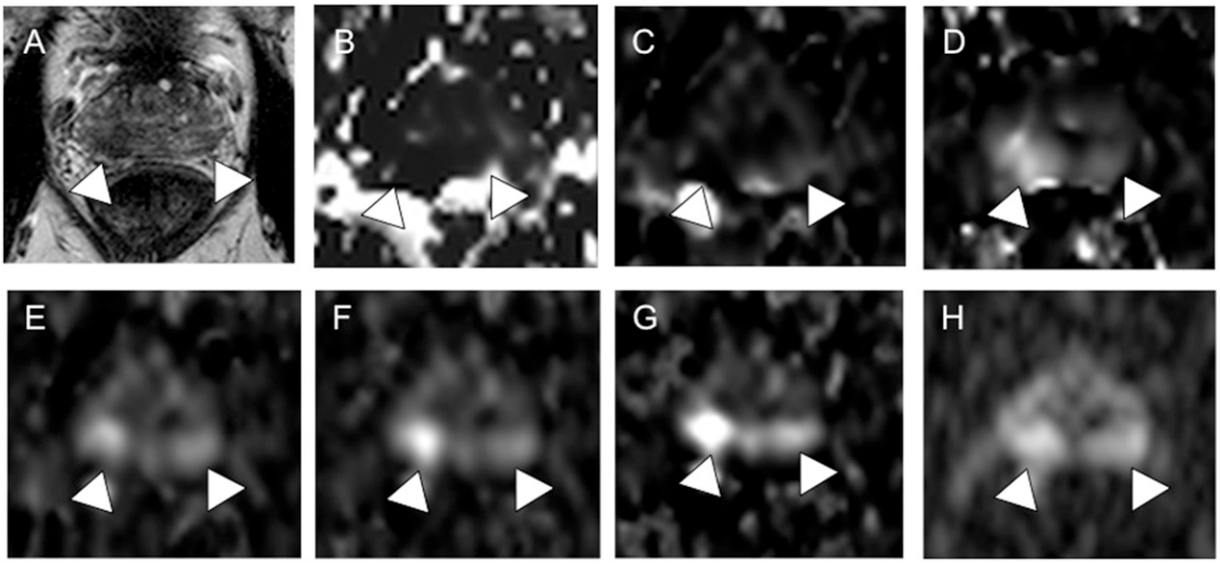

Although $cDWI_{0–100}$ and $cDWI_{0–500}$ obtained high CR, they showed poor image quality for various items for visual qualitative assessment. Also, a comparison of interobserver agreement for all seven protocol methods showed that the protocols using computed DWI generated from *b*-values with 0 and $<500\,s\,mm^{-2}$ showed relatively low κ values. This might be because that not only signals of cancerous lesion but also signals of normal prostate parenchyma were weakened and embedded in the background signal at those *b*-values. It is known that the initial decrease in signal intensities at low *b*-values is steeper than the more gradual attenuation of signals at higher *b*-values.[19] ADCs calculated from low *b*-values are prone to be larger, thus, computed signal based on an monoexponential model would be lower. As for diagnostic capability, Az of computed DWI generated from *b*-values with 0 and $<500\,s\,mm^{-2}$ was lower than that of other DW images. These are likely to be the result of their poor image quality. Even with a less strict evaluation, signals of relatively small cancers tend to be weaker on cDWI generated from *b*-values $<500\,s\,mm^{-2}$. This can be assumed to be the major reason that the sensitivities of $cDWI_{0–100}$ and $cDWI_{0–500}$ were lower than those of other images.

It should be noted that computed DWI does not provide information equivalent to a measured DWI image at the same *b*-value. Increasing *b*-value in measured DWI increases the motion sensitivity to slow tissue water diffusion components and reduces the microcirculation effect. However, on the other hand, computed DWI merely combines information from a set of images acquired with lower *b*-values. Increasing the *b*-value should therefore only be regarded as a way of enhancing the CR between areas with different ADCs.[20] According to the previous report,[21] a combination of *b*-values strongly influences the calculated ADCs. They also suggested that removing low *b*-values reduces the perfusion contamination of the diffusion signal and ADCs approach the biexponentially calculated Ds, thus, care should be taken when ADC calculation includes low *b*-values. Also, using low *b*-values, which are perfusion sensitive, may thus not be suitable for computing high *b*-value DW images. Our study outcomes suggest that *b*-value combinations with $b \geq 10\,s\,mm^{-2}$ and $b \geq 500\,s\,mm^{-2}$, as well as $b = 0\,s\,mm^{-2}$ and $b = 1000\,s\,mm^{-2}$ are recommended for computation of DWI at *b*-value with $2000\,s\,mm^{-2}$.

cDWI images, could not produce a higher PCa diagnostic accuracy than did a measured DWI at *b*-value with $2000\,s\,mm^{-2}$ in this study. However, this result may be induced by the fact that the measured DWI at *b*-value with $2000\,s\,mm^{-2}$ obtained high-quality images owing to our MR system's configuration. cDWI technique would offer several advantages. One is that images with high *b*-values can be obtained regardless of the MR system's configuration. This contrasts with previous studies reporting that a shorter echo time (TE) is more likely to yield a higher SNR for DWI ($>1000\,s\,mm^{-2}$).[4,5] Whereas the achievable minimum TE for DWI acquisition depends on the performance of a gradient system; cDWI technique can make high *b*-value images maintain tissue SI without depending on TE.[18]

This study has a few limitations. First, we did not evaluate SNRs of each DWI. Because the parallel imaging technique was used for measured DWI and each cDWI in this study, we could not assess noise itself. Second, as the main aim of this study was to evaluate DW image quality and diagnostic capability for PCa, findings for ADC were not evaluated in this study. Third, a limited number of low *b*-values were used for computation DWI. Moreover, the lower and higher limits of *b*-values were included in this study. In

addition, the study population was relatively small, and staging and/or therapeutic effect prediction or assessments were not evaluated in this study. Therefore, we plan large prospective cohort studies for answering the above-mentioned limitations and to demonstrate the real significance of this new technique for management of patients with PCa in the near future.

In conclusion, for PCa detection, our findings suggest that combinations of *b*-values with 0 s mm^{-2} and <500 s mm^{-2} are not suitable to generate cDWI at *b*-value with 2000 s mm^{-2}. Care should be taken when computing DWI by using low *b*-values. The combinations of $b \geq 100$ s mm^{-2} and $b \geq 500$ s mm^{-2}, as well as $b = 0$ s mm^{-2} and $b = 1000$ s mm^{-2} were optimal in this study.

ACKNOWLEDGMENTS

We thank Tomoo Ito, MD, PhD, Masato Fujisawa, MD, PhD, Katsusuke Kyotani, RT, Yu Ueda, PhD, for their generous support in the data analysis. We also thank Tokunori Kimura, PhD, for his support in providing us with computed DWI software.

CONFLICTS OF INTEREST

Masao Yui, MS, and Yoshimori Kassai, MS, are employees of Toshiba Medical Systems Corporation.

FUNDING

Co-author Yoshiharu Ohno, MD, PhD, has a research grant from Toshiba Medical Systems.

REFERENCES

1. Koh DM, Collins DJ. Diffusion-weighted MRI in the body applications and challenges in oncology. *AJR Am J Roentgenol* 2007; **188**: 1622–35.
2. Ohno Y, Koyama H, Onishi Y, Takenaka D, Nogami M, Yoshikawa T, et al. Non-small cell lung cancer: whole-body MR examination for M-stage assessment—utility for whole-body diffusion-weighted imaging compared with integrated FDG PET/CT. *Radiology* 2008; **248**: 643–54. doi: 10.1148/radiol.2482072039
3. Choi EK, Kim JK, Choi HJ, Park SH, Park BW, Kim N, et al. Node-by-node correlation between MR and PET/CT in patients with uterine cervical cancer: diffusion-weighted imaging versus size-based criteria on T2WI. *Eur Radiol* 2009; **19**: 2024–32. doi: 10.1007/s00330-009-1350-5
4. Koh DM, Blackledge M, Padhani AR, Takahara T, Kwee TC, Leach MO, et al. Whole-body diffusion-weighted MRI: tips, tricks, and pitfalls. *AJR Am J Roentgenol* 2012; **199**: 252–62. doi: 10.2214/AJR.11.7866
5. Koh DM, Takahara T, Imai Y, Collins DJ. Practical aspects of assessing tumors using clinical diffusion-weighted imaging in the body. *Magn Reson Med Sci* 2007; **6**: 211–24.
6. Hoeks CM, Barentsz JO, Hambrock T, Yakar D, Somford DM, Heijmink SW, et al. Prostate cancer: multiparametric MR imaging for detection, localization, and staging. *Radiology* 2011; **261**: 46–66. doi: 10.1148/radiol.11091822
7. Metens T, Miranda D, Absil J, Matos C. What is the optimal *b* value in diffusion-weighted MR imaging to depict prostate cancer at 3T? *Eur Radiol* 2012; **22**: 703–9. doi: 10.1007/s00330-011-2298-9
8. Katahira K, Takahara T, Kwee TC, Oda S, Suzuki Y, Morishita S, et al. Ultra-high-*b*-value diffusion-weighted MR imaging for the detection of prostate cancer: evaluation in 201 cases with histopathological correlation. *Eur Radiol* 2011; **21**: 188–96. doi: 10.1007/s00330-010-1883-7
9. Ueno Y, Kitajima K, Sugimura K, Kawakami F, Miyake H, Obara M, et al. Ultra-high *b*-value diffusion-weighted MRI for the detection of prostate cancer with 3-T MRI. *J Magn Reson Imaging* 2013; **38**: 154–60. doi: 10.1002/jmri.23953
10. Blackledge MD, Leach MO, Collins DJ, Koh DM. Computed diffusion-weighted MR imaging may improve tumor detection. *Radiology* 2011; **261**: 573–81. doi: 10.1148/radiol.11101919
11. Blackledge M, Wilton B, Messiou C, Koh D-M, Leach MO, Collins DJ. Computed diffusion weighted imaging (cDWI) for improving imaging contrast. Abstract 4005. In: Proceedings of the International Society for Magnetic Resonance in Medicine. Berkeley, CA: International Society for Magnetic Resonance in Medicine; 2009.
12. Blackledge M, Collins DJ, Koh DM, Leach MO. Signal to noise ratio of high *b*-value diffusion weighted images is improved using computed diffusion weighted imaging. Abstract 4707. In: Proceedings of the International Society for Magnetic Resonance in Medicine. Berkeley, CA: International Society for Magnetic Resonance in Medicine; 2010.
13. Ueno Y, Takahashi S, Kitajima K, Kimura T, Aoki I, Kawakami F, et al. Computed diffusion-weighted imaging using 3-T magnetic resonance imaging for prostate cancer diagnosis. *Eur Radiol* 2013; **23**: 3509–16. doi: 10.1007/s00330-013-2958-z
14. Akin O, Sala E, Moskowitz CS, Kuroiwa K, Ishill NM, Pucar D, et al. Transition zone prostate cancers: features, detection, localization, and staging at endorectal MR imaging. *Radiology* 2006; **239**: 784–92.
15. Kitajima K, Kaji Y, Kuroda K, Sugimura K. High *b*-value diffusion-weighted imaging in normal and malignant peripheral zone tissue of the prostate: effect of signal-to-noise ratio. *Magn Reson Med Sci* 2008; **7**: 93–9.
16. Kitajima K, Kaji Y, Fukabori Y, Yoshida K, Suganuma N, Sugimura K. Prostate cancer detection with 3 T MRI: comparison of diffusion-weighted imaging and dynamic contrast-enhanced MRI in combination with T2-weighted imaging. *J Magn Reson Imaging* 2010; **31**: 625–31. doi: 10.1002/jmri.22075
17. Kundel HL, Polansky M. Measurement of observer agreement. *Radiology* 2003; **228**: 303–8.
18. Kimura T, Machii Y. Computed diffusion weighted imaging under Rician noise distribution. Abstract 3574. In: Proceedings of the International Society for Magnetic Resonance in Medicine. Berkeley, CA: International Society for Magnetic Resonance in Medicine; 2012.
19. Koh DM, Collins DJ, Orton MR. Intravoxel incoherent motion in body diffusion-weighted MRI: reality and challenges. *AJR Am J Roentgenol* 2011; **196**: 1351–61. doi: 10.2214/AJR.10.5515
20. Maas MC, Fütterer JJ, Scheenen TW. Quantitative evaluation of computed high B value diffusion-weighted magnetic resonance imaging of the prostate. *Invest Radiol* 2013; **48**: 779–86. doi: 10.1097/RLI.0b013e31829705bb
21. Nilsen LB, Fangberget A, Geier O, Seierstad T. Quantitative analysis of diffusion-weighted magnetic resonance imaging in malignant breast lesions using different b value combinations. *Eur Radiol* 2013; **23**: 1027–33. doi: 10.1007/s00330-012-2687-8